PAPER

Monitoring nanoparticle dissolution *via* fluorescence-colour shift†

Christian Ritschel,[a] Joanna Napp, [b,c] Frauke Alves [*b,c] and Claus Feldmann [*a]

$[La(OH)]^{2+}[ICG]^{-}_2$ and $[La(OH)]^{2+}_2[PTC]^{4-}$ inorganic–organic hybrid nanoparticles (IOH-NPs) with indocyanine green (ICG) and perylene-3,4,9,10-tetracarboxylate (PTC) as fluorescent dye anions are used for emission-based monitoring of the dissolution of nanoparticles. Whereas ICG shows a deep red emission in the solid $[La(OH)]^{2+}[ICG]^{-}_2$ IOH-NPs, the emission of PTC in the solid $[La(OH)]^{2+}_2[PTC]^{4-}$ IOH-NPs is completely quenched due to π-stacking. After nanoparticle dissolution, the emission of freely dissolved ICG is weak, whereas freely dissolved PTC shows intense green emission. We report on the synthesis of IOH-NPs and nanoparticle characterization as well as on the fluorescence properties and how to avoid undesirable energy transfer between different fluorescent dyes. The emission shift from red (intact solid nanoparticles) to green (freely dissolved dye anions), indicating nanoparticle dissolution, is shown for aqueous systems and verified *in vitro*. Based on this first proof-of-the-concept, the IOH-NP marker system can be interesting to monitor nanoparticle dissolution in cells and tissues of small animals and to evaluate cell processes and/or drug-delivery strategies.

Introduction

Optical imaging (OI) has emerged as a cost-effective and versatile method for biomedical monitoring and is used to visualize and distinguish cellular compartments and tissues as well as to study active cellular processes.[1] Although OI is also applied in human medicine in the meantime, the penetration depth has made the method indispensable, especially, for cellular studies and *in vivo* studies of small animals (*e.g.*, mice, rats).[2] More recently, novel light-microscopic techniques, such as stimulated emission depletion (STED) or stochastic optical reconstruction microscopy (STORM),[3] have significantly expanded the options for OI. Specific markers with suitable fluorescence characteristics (*e.g.*, long-wavelength emission), sufficient physiological and photochemical stability, and high biocompatibility are essential for the success of OI.[1–3] For this purpose, a variety of molecular fluorescent dyes (most often derivatives of rhodamine, cyanine, squaraine, porphyrin, phthalocyanine, *etc.*)[4] have been suggested and attached in

different ways to carrier molecules or carrier structures (*e.g.*, silica, metal–organic frameworks, and carbon species).[5] Alternatively, fluorescent nanoparticles, such as quantum dots (*e.g.* CdSe@ZnS), plasmonic metal nanoparticles (*e.g.* Au), or up-converting nanoparticles (*e.g.*, $NaYF_4$:Er,Yb) have been widely used and are characterized by higher chemical and photochemical stability as compared to molecular fluorescent dyes.[5a,6]

Optical detection is usually related to a change in intensity rather than a change in wavelength and colour.[5–7] In some cases, the change in the fluorescence intensity was used to the point of an on–off or off–on behaviour. Such fluorescent nanoparticles have been exploited, for example, to study cellular uptake, drug delivery, drug release, and all kinds of sensing effects (*e.g.*, the detection of metal ions and the detection of molecules such as carbohydrates or antibodies), which can be partly performed in real time.[1,5–7] However, a change in the emission intensity has the disadvantage of being concentration dependent, which either requires distinct on–off/off–on characteristics or normalization of the emission intensity on a suitable reference. In this regard, changing the emission colour as a response to a certain effect or parameter would be much more effective. However, such a wavelength shift is more complex with regard to the selection of fluorescence markers and has only been reported in a few cases to date.[8]

Aiming at fluorescence-based monitoring of the dissolution of nanoparticles, and specifically, differentiation of the intact solid nanoparticles and the homogeneous solution after nanoparticle dissolution, we examined different strategies involving

aInstitute for Inorganic Chemistry, Karlsruhe Institute of Technology (KIT), Engesserstrasse 15, 76131 Karlsruhe, Germany. E-mail: claus.feldmann@kit.edu
bUniversity Medical Center Goettingen (UMG), Institute for Diagnostic and Interventional Radiology, Robert Koch Str. 40, 37075 Goettingen, Germany
cMax Planck Institute for Multidisciplinary Sciences, Translational Molecular Imaging, Hermann-Rein-Strasse 3, 37075 Goettingen, Germany.
E-mail: falves@gwdg.de
†Electronic supplementary information (ESI) available: Details regarding the analytical techniques and further data related to the material characterization of the IOH-NPs. See DOI: https://doi.org/10.1039/d2nr03078k

two different fluorescent dyes. This resulted in several limitations, whereof an undesirable energy transfer disturbs the intended fluorescence features most often. We are now successful with a mixture of $[La(OH)]^{2+}[ICG]^-_2$ and $[La(OH)]^{2+}_2[PTC]^{4-}$ inorganic–organic hybrid nanoparticles (IOH-NPs) (ICG: indocyanine green, PTC: perylene-3,4,9,10-tetracarboxylate), which show an emission shift from red (intact nanoparticles in aqueous suspension) to green (aqueous solution of freely dissolved fluorescent dyes) upon dissolution. This system of fluorescence markers – including synthesis, nanoparticle characterization, and proof-of-concept of the fluorescence-colour shift in the first *in vitro* studies – is shown here for the first time.

Experimental section

Synthesis

$[La(OH)]^{2+}[ICG]^-_2$ **IOH-NPs.** 39.5 mg (0.05 mmol) of Na(ICG) (abcr) was dissolved in 60 mL of water. In addition, 18.5 mg (0.05 mmol) of $LaCl_3 \cdot 7H_2O$ (Sigma-Aldrich, 99.9%) was dissolved in 0.5 mL of water and injected into the aforementioned ICG solution. The as-prepared $[La(OH)]^{2+}[ICG]^-_2$ IOH-NPs were separated by centrifugation (25 000 rpm, 15 min) and purified three times by redispersion/centrifugation in/from water. Finally, aqueous suspensions or dried powder samples were obtained.

$[La(OH)]^{2+}_2[PTC]^{4-}$ **IOH-NPs.** 6.3 mg (0.016 mmol) of perylene-3,4,9,10-tetracarboxylic dianhydride (PTCDA, abcr, 98%) was dissolved in 25 mL of 10 mmol L^{-1} NaOH by heating to 95 °C. After neutralisation with HCl (10 mmol L^{-1}), 15 mL of ethanol was added. Thereafter, 9.3 mg (0.025 mmol) of $LaCl_3 \cdot 7H_2O$ (Sigma-Aldrich, 99.9%), dissolved in 0.5 mL of water, was injected at 95 °C into the aforementioned PTCDA solution. After cooling, the as-prepared $[La(OH)]^{2+}_2[PTC]^{4-}$ IOH-NPs were separated by centrifugation (10 000 rpm, 15 min) and purified three times by redispersion/centrifugation in/from water. Finally, aqueous suspensions or dried powder samples were obtained.

On the other hand, $[La(OH)]^{2+}_2[PTC]^{4-}$@$LaPO_4$ core–shell IOH-NPs can be prepared (see the ESI†).

Analytical techniques

Details regarding sample preparation and analytical equipment are described in the ESI.†

In vitro studies

Cell cultures. The immortalized and adherent mouse alveolar macrophage cell line MH-S (CRL-2019, ATCC) was cultivated at 37 °C under a humidified atmosphere of 5% CO_2 in a complete RPMI medium supplemented with 10% fetal calf serum (FCS) and 0.05 mM 2-mercaptoethanol.

Incubation with IOH-NPs. MH-S cells were plated on a 35 mm μ-dish equipped with a polymer coverslip bottom (IBIDI), at a concentration of ~15 000 cells per cm^2 in 1 mL of cell culture medium. Cells were allowed to attach overnight.

On the next day, the macrophages were supplemented with 1 mL of medium, containing 50 μg mL^{-1} of the $[La(OH)]^{2+}[ICG]^-_2$ and $[La(OH)]^{2+}_2[PTC]^{4-}$ IOH-NPs.

Microscopy and image analysis. A Leica SP5 confocal laser-scanning microscope was used for imaging. Time-resolved imaging was started after 5.5 h of incubation, and images were recorded every other hour. A single image was recorded after 20 h of incubation with the IOH-NPs. ICG was excited at 633 nm (the highest available excitation wavelength) and the emitted fluorescence was monitored at 643–800 nm; PTC was excited at 514 nm and the emitted fluorescence was monitored at 524–574 nm. Additionally, cell autofluorescence was recorded at 458 nm for excitation and 468–518 nm for emission. The confocal images were processed using ImageJ (available by ftp at zippy.nimh.nih.gov or **https://rsb.info.nih.gov/nih-imageJ**, developed by W. Rasband, National Institutes of Health, U.S.).[9]

Results and discussion

Material concept and selection of fluorescent dyes

Aiming at nanoparticles for multimodal imaging and/or drug delivery, we have developed the concept of inorganic–organic hybrid nanoparticles (IOH-NPs).[10] These IOH-NPs are characterized by a saline composition with an inorganic cation and a functional organic anion. The functional organic anion can be a fluorescent dye and/or a pharmaceutical drug, which contains a phosphate, sulfonate, or carboxylate group. Together with a suitable inorganic cation, the functional organic anion forms an insoluble saline compound in water. Specific examples of fluorescent IOH-NPs, for instance, are $[Gd(OH)]^{2+}_2[DB71]^{4-}$, $[ZrO]^{2+}[FMN]^{2-}$, $[GdO]^+[ICG]^-$, or $[Gd(OH)]^{2+}_2[EB]^{4-}$ (DB71: direct blue 71, FMN: flavin mononucleotide, ICG: indocyanine green, and EB: Evans blue) showing blue, green, red, and infrared emission, respectively.[11] The specific advantages of the IOH-NPs comprise an aqueous synthesis, a simple material composition, an unprecedented high dye load (70–85 wt% of the total nanoparticle mass), and variability with regard to the selection of the dye anion. Due to the high dye load and the respective great number of luminescent centers per nanoparticle, the IOH-NPs, on the one hand, show intense emission, and on the other hand, have good photostability. The high number of luminescent centers per nanoparticle also guarantees a sufficient emission intensity even if the luminescence efficiency of the respective dye anion is limited or if the size of the IOH-NPs upon dissolution becomes smaller.[11]

To monitor the dissolution of the IOH-NPs based on their fluorescence, a careful selection of suitable fluorescent dyes is essential. In this regard, we have evaluated about 50 different fluorescent dyes that are compatible with the IOH-NP concept. All these fluorescent IOH-NPs, however, showed only a single emission, so a particle dissolution only resulted in a decrease in the emission, which is much less indicative than a fluorescence-colour shift. Such a colour shift, however, requires

the use of two different fluorescent dyes. The first dye should preferentially only emit in the solid nanoparticle but not show emission in solution, whereas the emission of the second dye should be quenched in the solid nanoparticle but be intense in solution. Due to the dilution in the solution, moreover, the second dye must exhibit a much more intense emission than the first dye. In addition to this default, further parameters need to be considered. Thus, long-wavelength excitation and emission are required in regard to the penetration depth in biological systems. Finally, energy transfer and/or overlapping emission of the fluorescent dyes need to be avoided in order to observe two different emission colours.

Although we have examined various combinations of dyes, an energy transfer between the two dyes could not be suppressed completely, so either significant fluorescence quenching or only a mixed emission colour of the two dyes was observed. The fact that the dyes are spatially close together with a high concentration in the nanoparticle volume, of course, favours the undesired energy transfer in comparison with the freely dissolved dyes in the solution. These restrictions were finally solved by two measures. First of all, the selection of the fluorescent dyes was most important. Here, we have used indocyanine green (ICG) as a first and perylene-3,4,9,10-tetracarboxylate (PTC) as a second dye (Fig. 1). Both are anionic and chemically fit with the concept of the IOH-NPs.[10] ICG as the first dye is known for its weak deep-red emission.[12] ICG is clinically approved and employed in a wide range of medical imaging and diagnostic procedures but most often as an absorptive dye (e.g. in histology) since its emission is weak.[13] Due to the high ICG-load in IOH-NPs, however, the deep-red emission is even visible in suspension to the naked eye. Subsequent to the dissolution of the IOH-NPs, the emission of the free $[ICG]^-$ can be expected to be negligible. Perylene tetracarboxylate (PTC) was selected as the second dye. Such perylene-type dyes are generally known for their extre-

mely intense emission with high luminescence efficiency[14] and also show good biocompatibility.[15] Due to the π-stacking of the molecules and the so-called aggregation-caused quenching (ACQ) effect, the emission of PTC is completely quenched in the solid nanoparticles. After the dissolution of the IOH-NPs, however, the freely dissolved $[PTC]^{4-}$ shows a bright green emission.

In addition to the selection of the fluorescent dyes – as a second measure – it turned out to be essential not to combine both dyes in one nanoparticle but to use mixed suspensions with both types of IOH-NPs (Fig. 1). For such IOH-NP mixtures, the expected fluorescence-colour shift from red (solid nanoparticles) to green (dissolved nanoparticles) was successfully observed. In the case of IOH-NPs containing a combination of ICG and PTC, in contrast, two disadvantageous effects were observed. First, these IOH-NPs with combined dyes, again, show an undesired energy transfer with emission of ICG upon excitation of PTC (ESI: Fig. S1a†). Moreover and even more important, combining ICG and PTC in a single IOH-NP disturbs the π-stacking of PTC, so the PTC emission is not quenched in the solid IOH-NPs (ESI: Fig. S1b†). Overall, this points to the feasibility of the concept of mixing two different types of IOH-NPs, each of them containing only a single fluorescent dye.

Nanoparticle synthesis and characterization

The synthesis of fluorescent IOH-NPs follows our previous work, which is characterized by water-based precipitation at room temperature (Fig. 1).[10] In order to obtain insoluble IOH-NPs in water, the fluorescent dye anions $[ICG]^-$ and $[PTC]^{4-}$ were combined with La^{3+} as an inorganic cation, which – depending on the pH level and the coordinative situation of the respective dye anion – is present as the $[La(OH)]^{2+}$ or $[LaO]^+$ cation in the IOH-NPs. Accordingly, a concentrated aqueous solution of $LaCl_3 \cdot 7H_2O$ was injected into solutions of Na(ICG) or Na_4(PTC) (Fig. 2). In regard to PTC, the starting material perylene-3,4,9,10-tetracarboxylic dianhydride (PTCDA) needs to be converted from the cyclic ester to the tetraanion by alkaline treatment with aqueous NaOH. Following the model
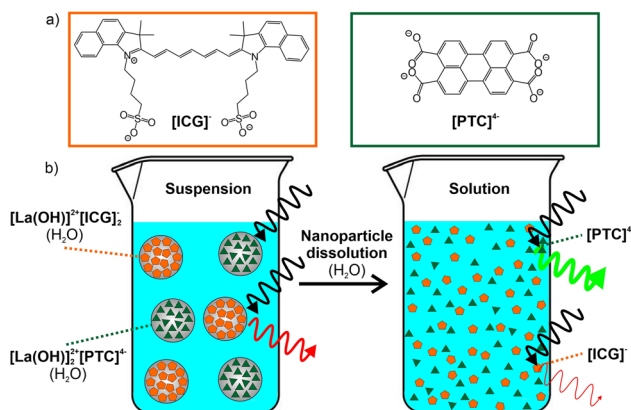
Fig. 1 Scheme illustrating the fluorescence-colour shift of IOH-NPs with indocyanine green (ICG) and perylene tetracarboxylate (PTC) as fluorescent dyes showing a deep red ICG-based emission in the solid nanoparticle and a green emission after IOH-NP dissolution: (a) composition of the $[ICG]^-$ and the $[PTC]^{4-}$ anion and (b) fluorescence of the aqueous IOH-NP suspension and freely dissolved dyes in solution.
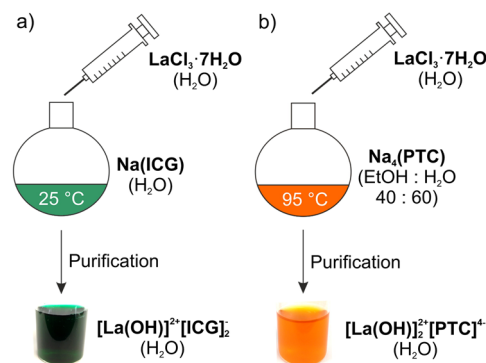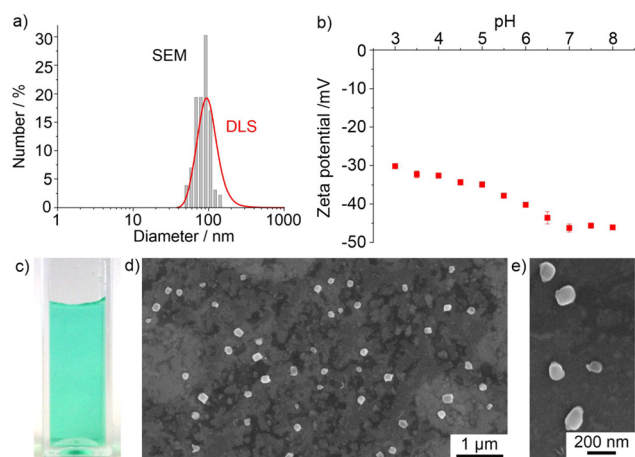

Fig. 2 Schematic aqueous synthesis of (a) $[La(OH)]^{2+}[ICG]^-_2$ IOH-NPs and (b) $[La(OH)]^{2+}_2[PTC]^{4-}$ IOH-NPs.

of LaMer and Dinegar,[16] particle nucleation was performed by injection with vigorous stirring.

After certain purification to remove the remaining starting materials and salts, $[La(OH)]^{2+}[ICG]^-{}_2$ IOH-NPs with 90% ICG per total nanoparticle mass were obtained as a colloidally stable, deep green aqueous suspension (Fig. 2; ESI: Fig. S2–S5†). In contrast, the as-obtained orange suspension of the $[La(OH)]^{2+}{}_2[PTC]^{4-}$ IOH-NPs (with 60% PTC per total nanoparticle mass) only resulted in suspensions with low colloidal stability with rapid Ostwald ripening, causing very large particles (5–10 μm) after about 1 hour (ESI: Fig. S6†). Since the polar carboxylate groups of the PTC anion coordinate with the cation, this finding can be ascribed to the non-polar particle surface established by the perylene backbone. To decrease the particle size and to increase the colloidal stability, two options are possible. Thus, particle nucleation can be performed at an elevated temperature (95 °C) to promote particle nucleation. Alternatively, the $[La(OH)]^{2+}{}_2[PTC]^{4-}$ IOH-NPs can also be modified using a $LaPO_4$ shell, which was established immediately after the nucleation process (ESI: Fig. S7–S13†). Aqueous suspensions of both $[La(OH)]^{2+}{}_2[PTC]^{4-}$ IOH-NPs prepared at 95 °C and core–shell-type $[La(OH)]^{2+}{}_2[PTC]^{4-}@LaPO_4$ IOH-NPs are colloidally stable over several weeks (Fig. 3c and 4c; ESI: Fig. S11†).

The particle size and particle size distribution of the as-prepared $[La(OH)]^{2+}[ICG]^-{}_2$ and $[La(OH)]^{2+}{}_2[PTC]^{4-}$ IOH-NPs were characterized by dynamic light scattering (DLS) and scanning electron microscopy (SEM). Since nanoparticles in water typically exhibit an expanded, rigid layer of adsorbed H_2O molecules, the primary particle diameter was examined *via* DLS after dispersion of the IOH-NPs in diethylene glycol (DEG), which is known for its excellent stabilization of nanoparticles.[17] Accordingly, DLS shows mean diameters of 103 ± 13 nm ($[La(OH)]^{2+}[ICG]^-{}_2$) and 73 ± 12 nm ($[La(OH)]^{2+}{}_2[PTC]^{4-}$) (Fig. 3a and 4a). Based on a statistical evaluation of >100 par-
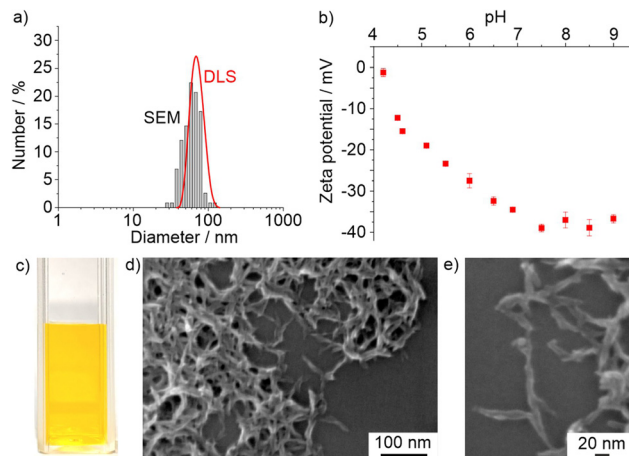
Fig. 4 Particle characterization of the $[La(OH)]^{2+}{}_2[PTC]^{4-}$ IOH-NPs: (a) particle size and particle size distribution according to DLS (in DEG) and SEM (statistical evaluation of 110 nanoparticles); (b) zeta potential analysis; (c) photo of the aqueous suspension; and (d and e) SEM images at different levels of magnification.

ticles on SEM images, mean diameters of 84 ± 40 nm ($[La(OH)]^{2+}[ICG]^-{}_2$) and 61 ± 15 nm ($[La(OH)]^{2+}{}_2[PTC]^{4-}$) were determined (Fig. 3a, d and 4a, d). The different values of DLS and SEM relate to the larger hydrodynamic diameter obtained by DLS. Whereas a spherical shape is observed for $[La(OH)]^{2+}[ICG]^-{}_2$ (Fig. 3e), rod-shaped particles are obtained for $[La(OH)]^{2+}{}_2[PTC]^{4-}$ (Fig. 4e). This finding can be again ascribed to the π-stacking of the PTC anion. Both types of IOH-NPs show negative surface charging as indicated by zeta potentials of −35 to −45 mV at pH 5–9 (Fig. 3b and 4b). An even higher negative charging was observed for the $[La(OH)]^{2+}{}_2[PTC]^{4-}@LaPO_4$ core–shell IOH-NPs with a zeta potential of −40 mV over the complete pH range (ESI: Fig. S11†), which also confirms the formation of the $LaPO_4$ shell.

To prove the chemical composition of the $[La(OH)]^{2+}[ICG]^-{}_2$ and $[La(OH)]^{2+}{}_2[PTC]^{4-}$ IOH-NPs, different analytical methods were used. First of all, X-ray powder diffraction (XRD) indicates the nanoparticles to be essentially non-crystalline, which was frequently observed for other IOH-NPs as well (ESI: Fig. S2 and S7†).[10] Only $[La(OH)]^{2+}{}_2[PTC]^{4-}$ shows few, low-intensity Bragg peaks, which can be ascribed to the π-stacking of the PTC anions (ESI: Fig. S7†). Fourier-transform infrared (FT-IR) spectroscopy reveals the presence of ICG and PTC in the IOH-NPs (ESI: Fig. S3 and S8†). Thus, the spectra of the IOH-NPs are well in agreement with Na(ICG) and $Na_4(PTC)$ as the starting materials. Energy dispersive X-ray spectroscopy (EDXS) confirmed the presence of lanthanum in the IOH-NPs. Finally, the cation-to-anion ratio was confirmed by total organic combustion analysis, including thermogravimetry (TG) and elemental analysis (EA) (ESI: Fig. S4 and S9†).

Fig. 3 Particle characterization of the $[La(OH)]^{2+}[ICG]^-{}_2$ IOH-NPs: (a) particle size and particle size distribution according to DLS (in DEG) and SEM (statistical evaluation of 130 nanoparticles); (b) zeta potential analysis; (c) photo of the aqueous suspension; and (d and e) SEM images at different levels of magnification.

Fluorescence properties
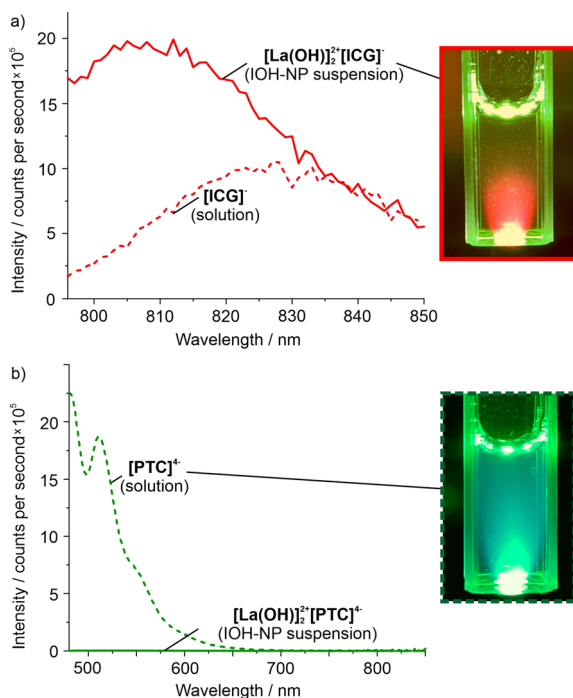
In regard to the fluorescence properties of the IOH-NPs, the red emission of aqueous suspensions of $[La(OH)]^{2+}[ICG]^-{}_2$ is

visible even to the naked eye upon excitation, for instance, with a blue-light-emitting LED or a halogen lamp with glass fibre (Fig. 5a; greenish scattered light due to the deep green colour of $[La(OH)]^{2+}[ICG]^-_2$, compare Fig. 3c). Excitation and emission were quantified by photoluminescence spectroscopy. Accordingly, $[La(OH)]^{2+}[ICG]^-$ IOH-NPs show strong visible absorption (600–800 nm) and deep-red emission (800–850 nm) with a maximum at 811 nm (Fig. 5a; ESI: Fig. S5†). In comparison, an aqueous solution of Na(ICG) with a similar ICG concentration to the IOH-NP suspension was examined. Although the emission of the $[La(OH)]^{2+}[ICG]^-$ suspension and that of the ICG solution are, in principle, similar, the IOH-NPs interestingly show a 2–3 times more intense emission (Fig. 5a). This finding can be attributed to the quasi-infinite number of fluorescent centers in the nanoparticle volume.
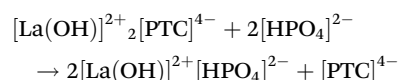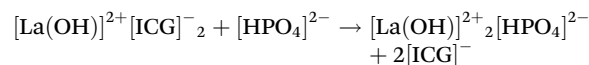
For the $[La(OH)]^{2+}_2[PTC]^{4-}$ IOH-NPs, as expected, no emission was observed for the aqueous suspensions due to the π-stacking of the PTC anions in the solid nanoparticles (Fig. 5b). Thus, emission spectra more-or-less show a zero line. In contrast, a solution of $Na_4(PTC)$ with a PTC concentration similar to that of the IOH-NPs shows strong absorption at 350–500 nm and very intense emission at 500–700 nm with a maximum at 517 nm (Fig. 5b; ESI: Fig. S10, S12 and S13†).

After examination of the individual $[La(OH)]^{2+}[ICG]^-_2$ and $[La(OH)]^{2+}_2[PTC]^{4-}$ IOH-NPs, the fluorescence features 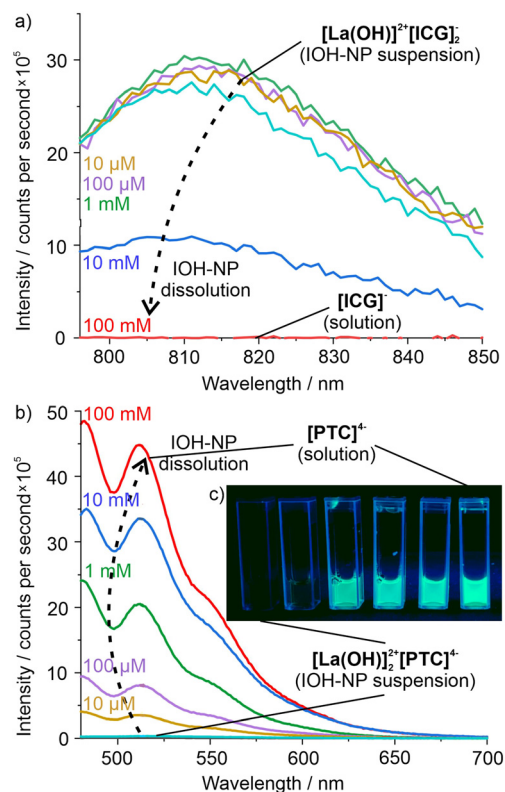of aqueous suspensions containing both types of IOH-NPs were studied. The dissolution of the IOH-NPs was initiated by redispersion of the IOH-NPs in a phosphate buffer at pH 7 at concentrations of 10 μM, 100 μM, 1.0 mM, 10 mM, and 100 mM phosphate (Fig. 6). In the presence of phosphate, ICG and PTC are released due to the stronger complexion of lanthanum by phosphate in comparison with the sulfonate group of ICG or the carboxylate group of PTC (see Fig. 1a) according to the following equations:

$$[La(OH)]^{2+}[ICG]^-_2 + [HPO_4]^{2-} \rightarrow [La(OH)]^{2+}_2[HPO_4]^{2-} + 2[ICG]^-$$

$$[La(OH)]^{2+}_2[PTC]^{4-} + 2[HPO_4]^{2-} \rightarrow 2[La(OH)]^{2+}[HPO_4]^{2-} + [PTC]^{4-}$$

The release of ICG and PTC is slow due to slow equilibration and due to the size of the IOH-NPs (60–80 nm). Since phosphate is omnipresent in the blood, cells, and tissues, phosphate-induced dissolution can be considered to mimic the particle dissolution under biological conditions with about 1.5 mM phosphate in the human blood serum[18] and up to 100 mM as the intracellular phosphate level.[19]

The photoluminescence spectra recorded for the different samples confirm the aforementioned course of the emission
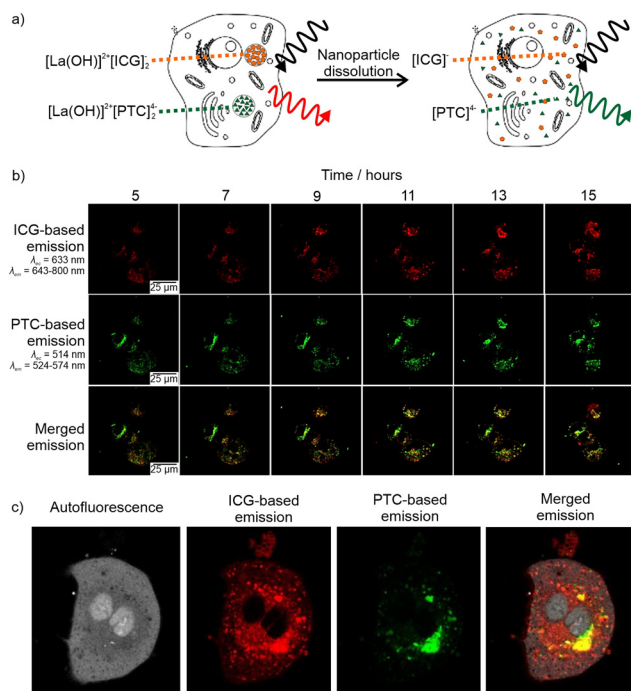

Fig. 5 Emission of the individual IOH-NPs: (a) $[La(OH)]^{2+}_2[ICG]^-_2$ suspension (with photo) and a Na(ICG) solution as a reference and (b) [La(OH)]$^{2+}_2[PTC]^{4-}$ suspension and a Na$_4$(PTC) solution (with photo) as a reference. All samples in demineralized water (spectra recorded with λ_{exc}(ICG): 781 nm, λ_{exc}(PTC): 465 nm; photos with blue-light-emitting LED for excitation).

Fig. 6 Emission of mixed $[La(OH)]^{2+}[ICG]^-_2/[La(OH)]^{2+}_2[PTC]^{4-}$ IOH-NPs in phosphate buffer at concentrations of 10 μM, 100 μM, 1.0 mM, 10 mM, and 100 mM: (a) ICG-related red emission and (b) PTC-related green emission (with a series of photos). All samples in demineralized water (λ_{exc}(ICG): 781 nm, λ_{exc}(PTC): 465 nm).

intensity. Thus, the ICG emission decreases slowly upon dissolution of the $[La(OH)]^{2+}[ICG]^-_2$ IOH-NPs (Fig. 6a). In contrast, the $[La(OH)]^{2+}_2[PTC]^{4-}$ IOH-NPs show no emission prior to beginning dissolution. After addition of the phosphate buffer, the PTC-related green emission increases significantly with the phosphate concentration as well as the proceeding IOH-NP dissolution and PTC release into the solution (Fig. 6b). In sum, the nanoparticle dissolution can be indeed followed by a fluorescence-colour shift from red (nanoparticle suspension) to green (solution).

After examining the dissolution of individual IOH-NPs and a mixture of both IOH-NPs, first *in vitro* studies were performed as a proof-of-concept (Fig. 7a). To this concern, mixed suspensions with both $[La(OH)]^{2+}[ICG]^-_2$ and $[La(OH)]^{2+}_2[PTC]^{4-}$ IOH-NPs were cultivated with MH-S mouse alveolar macrophages at 37 °C for up to 15 h. Similar to the suspensions, thereafter, the red and/or green emission was detected within the cells by fluorescence microscopy.

Time-dependent micrographs over 15 hours (Fig. 7b) as well as detailed micrographs (Fig. 7c) show both the red emission of ICG and the green emission of PTC, indicating the uptake of both types of IOH-NPs into the MH-S cells.

Interestingly, red and green emissions are continuously visible over the whole observed time range. This is different from the aforementioned suspensions with individual or mixed IOH-NPs (Fig. 5 and 6). This finding can be attributed to two effects. On the one hand, the metabolic degradation of ICG and PTC in cells can be considered to be different so that the dye concentration may differ from *ex vitro* aqueous suspensions. On the other hand, the freely dissolved ICG and PTC are not released out of the cells, so they remain in the cell, resulting in a lower dilution effect in comparison with the great volume of aqueous suspensions. Detailed micrographs after the incubation, nevertheless, indicate a more granular structure for the red-emitting areas than for the green-emitting areas, which is in agreement with the presence of intact $[La(OH)]^{2+}[ICG]^-_2$ IOH-NPs (Fig. 7c). In contrast, the green emission is more diffuse and the most intense at larger agglomerates of IOH-NPs (Fig. 7c), which points to the beginning of the dissolution of the $[La(OH)]^{2+}_2[PTC]^{4-}$ IOH-NPs.

Thus, particle dissolution can in principle also be monitored through *in vitro* cell-based assays based on a fluorescence-colour shift from red to green, which is here shown for the first time with $[La(OH)]^{2+}[ICG]^-_2$ and $[La(OH)]^{2+}_2[PTC]^{4-}$ IOH-NPs in macrophages. Additional studies are of course necessary to optimize and to fine-tune the relevant parameters and conditions. This will be even more interesting in combination with the evaluation of the time kinetics of different drug delivery systems, especially for the optimization of IOH-NPs that are loaded with certain pharmaceutical agents.

Conclusions and outlook

The dissolution of nanoparticles is followed based on a fluorescence-colour shift, which is easier to detect than a variation in the emission intensity. To this concern, $[La(OH)]^{2+}[ICG]^-_2$ and $[La(OH)]^{2+}_2[PTC]^{4-}$ inorganic–organic hybrid nanoparticles (IOH-NPs) with indocyanine green (ICG) and perylene-3,4,9,10-tetracarboxylate (PTC) as fluorescent dye anions were used for the first time. Whereas ICG shows a deep red emission in solid nanoparticles, the emission of PTC is completely quenched due to π-stacking in the solid state. After nanoparticle dissolution, the emission of ICG in the solution is weak, whereas freely dissolved PTC exhibits bright green emission. The shift of the emission colour during nanoparticle dissolution was evidenced for aqueous suspensions of individual IOH-NPs as well as for mixed suspensions with both types of IOH-NPs. The dissolution of the nanoparticles was initiated by the addition of phosphate in the concentration range of 10 μM to 100 mM, which mimics the phosphate level in the human blood serum (about 1.5 mM) or in cells (about 100 mM). As a first proof-of-concept, the fluorescence-colour shift from red (intact nanoparticles) to green (freely dissolved fluorescent dye anions) was also shown *in vitro* in a cell-based assay. With the simple synthesis and composition of the IOH-NPs as well as the possibility to monitor nanoparticle dis-

Fig. 7 Emission of mixed $[La(OH)]^{2+}[ICG]^-_2/[La(OH)]^{2+}_2[PTC]^{4-}$ IOH-NPs after incubation with MH-S macrophages (50 μg mL^{-1} of [La(OH)]$^{2+}$[ICG]$^-_2$ and [La(OH)]$^{2+}_2$[PTC]$^{4-}$): (a) scheme of IOH-NPs and emission prior and after dissolution, (b) fluorescence micrographs of a living macrophage over 15 hours of incubation with the IOH-NPs, and (c) detailed micrographs of an MH-S cell after 20 h of incubation demonstrating high IOH-NP uptake and intracellular, endosomal localisation of both ICG- and PTC-related fluorescence. Images show autofluorescence (λ_{exc}: 458 nm, λ_{exc}: 468–518 nm), ICG-related emission (λ_{exc}: 633 nm, λ_{exc}: 643–800 nm), PTC-related emission (λ_{exc}: 514 nm, λ_{exc}: 524–574 nm), and merged emission.

solution based on a shift of the emission colour, the system $[La(OH)]^{2+}[ICG]^{-}_2/[La(OH)]^{2+}_2[PTC]^{4-}$ can be of general relevance for optical imaging, including an evaluation of cell processes, the localization of nanoparticles, or visualisation of nanoparticle dissolution. Thereby, the here developed IOH-NPs are valuable tools to especially monitor and optimize novel drug delivery strategies using nanocarriers, *e.g.*, IOH-NPs for the remote delivery of appropriate dosage of drugs to targeted anatomical sites under controlled release.

Conflicts of interest

There are no conflicts to declare.

Acknowledgements

References

1 (a) S. Kunjachan, J. Ehling, G. Storm, F. Kiessling and T. Lammers, *Chem. Rev.*, 2015, **115**, 10907–10937; (b) T. L. Doane and C. Burda, *Chem. Soc. Rev.*, 2012, **41**, 2885–2911.

2 (a) M. Gao, F. Yu, C. Lv, J. Choo and L. Chen, *Chem. Soc. Rev.*, 2017, **46**, 2237–2271; (b) L. Nie and X. Chen, *Chem. Soc. Rev.*, 2014, **43**, 7132–7170.

3 S. W. Hell, S. J. Sahl, M. Bates, X. Zhuang, R. Heintzmann, M. J. Booth, J. Bewersdorf, G. Shtengel, H. Hess, P. Tinnefeld, A. Honigmann, S. Jakobs, I. Testa, L. Cognet, B. Lounis, H. Ewers, S. J. Davis, C. Eggeling, D. Klenerman, K. I. Willig, G. Vicidomini, M. Castello, A. Diaspro and T. Cordes, *J. Phys. D: Appl. Phys.*, 2015, **48**, 1–35.

4 (a) M. J. Schnermann, *Nature*, 2017, **551**, 176–177; (b) L. Yuan, W. Lin, K. Zheng, L. He and W. Huang, *Chem. Soc. Rev.*, 2013, **42**, 622–661.

5 (a) O. S. Wolfbeis, *Chem. Soc. Rev.*, 2015, **44**, 4743–4768; (b) C. Caltagirone, A. Bettoschi, A. Garau and R. Montis, *Chem. Soc. Rev.*, 2015, **44**, 4645–4671; (c) J. Wen, Y. Xu, H. Li, A. Lu and S. Sun, *Chem. Commun.*, 2015, **51**, 11346–11358.

6 (a) C. Lee, B. Lawrie, R. Pooser, K.-G. Lee, C. Rockstuhl and M. Tame, *Chem. Rev.*, 2021, **121**, 4743–4804; (b) K. D. Wegner and N. Hildebrandt, *Chem. Soc. Rev.*, 2015, **44**, 4792–4834.

7 (a) M. J. Mitchell, M. M. Billingsley, R. M. Haley, M. E. Wechsler, N. A. Peppas and R. Langer, *Nat. Rev. Drug Discovery*, 2021, **20**, 101–124; (b) Z. Fan, L. Sun, Y. Huang, Y. Wang and M. Zhang, *Nat. Nanotechnol.*, 2016, **11**, 388–394; (c) J. Tang, B. Kong, H. Wu, M. Xu, Y. Wang, Y. Wang, D. Zhao and G. Zheng, *Adv. Mater.*, 2013, **25**, 6569–6574; (d) T. O. McDonald, P. Martin, J. P. Patterson, D. Smith, M. Giardiello, M. Marcello, V. See, R. K. O'Reilly, A. Owen and S. Rannard, *Adv. Funct. Mater.*, 2012, **22**, 2469–2478; (e) A. Palma, L. A. Alvarez, D. Scholz, D. O. Frimannsson, M. Grossi, S. J. Quinn and D. F. O'Shea, *J. Am. Chem. Soc.*, 2011, **133**, 19618–19621.

8 (a) W. Zhao, Y. Zhao, Q. Wang, T. Liu, J. Sun and R. Zhang, *Small*, 2019, **15**, 1903060; (b) G. Shim, S. Ko, D. Kim, Q.-V. Le, G. T. Park, J. Lee, T. Kwon, H.-G. Choi, Y. B. Kim and Y.-K. Oh, *J. Controlled Release*, 2017, **267**, 67–79; (c) J. Tang, B. Kong, H. Wu, M. Xu, Y. Wang, Y. Wang, D. Zhao and G. Zheng, *Adv. Mater.*, 2013, **25**, 6569.

9 M. D. Bramoff, P. J. Magalhaes and S. J. Ram, *Biophoton. Internat.*, 2004, **11**, 36–42.

10 (a) M. Poß, E. Zittel, C. Seidl, A. Meschkov, L. Muñoz, U. Schepers and C. Feldmann, *Adv. Funct. Mater.*, 2018, **28**, 1801074; (b) M. Poß, R. J. Tower, J. Napp, L. C. Appold, T. Lammers, F. Alves, C.-C. Glüer, S. Boretius and C. Feldmann, *Chem. Mater.*, 2017, **29**, 3547–3554; (c) M. Poß, J. Napp, O. Niehaus, R. Pöttgen, F. Alves and C. Feldmann, *J. Mater. Chem. C*, 2015, **3**, 3860–3868.

11 (a) B. L. Neumeier, M. Khorenko, F. Alves, O. Goldmann, J. Napp, U. Schepers, H. M. Reichardt and C. Feldmann, *ChemNanoMat*, 2019, **5**, 24–45; (b) M. Poß, E. Zittel, A. Meschkov, U. Schepers and C. Feldmann, *Bioconjugate Chem.*, 2018, **29**, 2818–2828.

12 W. Pawlina and M. A. Ross, *Histology: A Text and Atlas*, Walters Kluwer, Philadelphia, 8th edn, 2020.

13 (a) D.-H. Li and B. D. Smith, *Chem. – Eur. J.*, 2021, **27**, 14535–11454; (b) Z. Starosolski, R. Bhavane, K. B. Ghaghada, S. A. Vasudevan, A. Kaay and A. Annapragada, *PLoS One*, 2017, **12**, e0187563.

14 Z. Chen, U. Baumeister, C. Tschierske and F. Wuerthner, *Chem. – Eur. J.*, 2007, **13**, 450–465.

15 (a) C. Kohl, T. Weil, J. Qu and K. Muellen, *Chem. – Eur. J.*, 2004, **10**, 5297–5310; (b) C. Minard-Basquin, T. Weil, A. Hohner, J. O. Raedler and K. Muellen, *J. Am. Chem. Soc.*, 2003, **125**, 5832–5838.

16 V. K. LaMer and R. H. J. Dinegar, *J. Am. Chem. Soc.*, 1950, **72**, 4847–4854.

17 R. Witter, M. Roming, C. Feldmann and A. S. Ulrich, *J. Colloid Interface Sci.*, 2013, **390**, 250–257.

18 V. K. Bansal, Serum Inorganic Phosphorus, in *Clinical Methods: The History, Physical, and Laboratory Examinations*, ed. H. K. Walker, W. D. Hall and J. W. Hurst, Butterworths, Boston, 3rd edn, 1990, ch. 198.

19 M. R. Thomas and E. K. O'Shea, *Proc. Natl. Acad. Sci. U. S. A.*, 2005, **102**, 9565–9570.